Applied Surface Science 410 (2017) 513–518

Contents lists available at ScienceDirect

Applied Surface Science

journal homepage: www.elsevier.com/locate/apsusc

Full Length Article

The effect of bulk/surface defects ratio change on the photocatalysis of TiO_2 nanosheet film

Fangfang Wang[a,1], Wenna Ge[b,c,1], Tong Shen[a], Bangjiao Ye[b,c], Zhengping Fu[a,*], Yalin Lu[a,d,e,**]

[a] CAS Key Laboratory of Materials for Energy Conversion, Department of Materials Science and Engineering, University of Science and Technology of China, Hefei 230026, People's Republic of China
[b] State Key Laboratory of Particle Detection and Electronics, University of Science and Technology of China, Hefei 230026, People's Republic of China
[c] Department of Modern Physics, University of Science and Technology of China, Hefei 230026, People's Republic of China
[d] Synergetic Innovation Center of Quantum Information & Stop Quantum Physics, University of Science and Technology of China, Hefei 230026, People's Republic of China
[e] National Synchrotron Radiation Laboratory, University of Science and Technology of China, Hefei 230026, Anhui, People's Republic of China

ARTICLE INFO

Article history:
Received 19 January 2017
Received in revised form 13 March 2017
Accepted 15 March 2017
Available online 19 March 2017

Keywords:
Bulk defect
Adsorb oxygen
Surface defect
Photocatalysis behaviors

ABSTRACT

The photocatalysis behavior of TiO_2 nanosheet array films was studied, in which the ratio of bulk/surface defects were adjusted by annealing at different temperature. Combining positron annihilation spectroscopy, EPR and XPS, we concluded that the bulk defects belonged to Ti^{3+} related vacancy defects. The results show that the separation efficiency of photogenerated electrons and holes could be significantly improved by optimizing the bulk/surface defects ratio of TiO_2 nanosheet films, and in turn enhancing the photocatalysis behaviors.

1. Introduction

As one of the most important semiconductor materials, TiO_2 nanomaterials have electronic band gaps larger than 3.0 eV and high absorption in the UV region, so their applications in photocatalytic are very distinguished [1]. The TiO_2 photocatalytic reaction principle can be represented as: Electrons will be activated from the valence band to the conduction band and produce electron-hole pairs when photons with the energy equal to or greater than the band gap of TiO_2 have been absorbed. Then, these electron-holes migrate to the surface and react with the chemicals adsorbed on the surface to decompose these chemicals. Universality, owing to the relation between the physical properties and the photocatalytic process is complicated, so photocatalytic efficiency is determined by many factors [2]: the light absorption coefficient, the electron-hole recombination rate, and the electron-hole induced reduction or oxidation rates on the surface. The larger surface area with a constant surface density of adsorbents, the faster surface photocatalytic reaction rates should be. Therefore, a larger specific surface area infers a higher photocatalytic activity. However, the surface is a defective site, so the larger the surface area also leads to the faster recombination of electron-hole. Moreover, the existence of bulk defects can play as charge carrier traps and result the recombination of electron-hole. Based on the above statements, the synergistic function of defects in surface and bulk to photocatalytic efficiency should be studied in details.

Kong et al. [3] showed that the separation efficiency of photogenerated electrons and holes could meaningfully be enhanced in TiO_2 powders when the relative concentration ratio between bulk defects and surface defects was decreased, which can obviously improve the photocatalytic efficiency. Some works have also studied the effect of the defects on the reactivity, electronic properties, electrostatic drift, ferromagnetism and adsorption–desorption with H_2O and O_2 of TiO_2 [4–15], however, the type of defects involved in these synergistic surface and bulk functions still need to be identified. In addition, the cooperation effect of surface and bulk defects in TiO_2 nanosheet arrays films [16–19], have not been

* Corresponding author.
** Corresponding author at: CAS Key Laboratory of Materials for Energy Conversion, Department of Materials Science and Engineering, University of Science and Technology of China, Hefei 230026, People's Republic of China.
E-mail addresses: fuzp@ustc.edu.cn (Z. Fu), yllu@ustc.edu.cn (Y. Lu).
[1] These authors contributed equally to this work.

http://dx.doi.org/10.1016/j.apsusc.2017.03.142
0169-4332/

reported too. These arrays can lead to improved photocatalysis efficiency or may be used as electron transfer layer in high efficient perovskite solar cells [16,20].

In this work, an anatase TiO_2 nanosheet array film is synthesized directly on a fluorine-doped tin oxide substrate via hydrothermal method. TiO_2 nanosheet films with different bulk/surface defect ratios were acquired by annealed at different temperature. Combining positron annihilation spectroscopy, EPR and XPS, we firstly conclude that the bulk defects are belonging to Ti^{3+} related vacancy defects. The redundant of adsorb oxygen which can see as the surface defects, were negative for the separation and migration of electron-hole and therefore reduced the photocatalytic activity. The results show that the separation efficiency of photogenerated electrons and holes could be significantly improved by controlling bulk/surface defects ratio of TiO_2 nanosheet, and in turn affected the photocatalysis behaviors.

2. Experimental

2.1. Sample preparation

The TiO_2 nanosheet array films exposed with the {116} facets were prepared following the hydrothermal method reported in our previous work [16]. The obtained films were annealed at different temperatures (300, 400 and 500 °C) for 2 h at normal atmosphere. Then the samples were cooled down to the room temperature naturally. The samples with annealing temperatures of 300 °C, 400 °C, 500 °C and the un-annealed sample are named as TiO_2-300, TiO_2-400, TiO_2-500 and $TiOF_2$, respectively.

2.2. Characterization

The morphology was analyzed by scanning electron microscopy (SEM, JSM-6700F). The purity and crystallinity were investigated using the X-Ray diffraction (XRD) with Cu-Kα radiation (Rigaku-TTR III). The X-ray photoelectron spectra (XPS) were obtained on Microtech, Twin Anode XR3E2 Spectrometer by using Al Ka radiation of 1486.6 eV as the X-ray source. Electron paramagnetic resonance measurements at X-band were carried out on a JES-FA200 spectrometer and the spectra were gained using electron paramagnetic resonance (JES-FA200) with xenon lamp as the excitation source. Photoluminescence emission spectra were characterized by fluorescence spectrophotometer (F-4600).

Photocurrent measurement was characterized in a three-electrode electrochemical cell with the electrochemical workstation (CHI660E, Shanghai Chenhua Device Company, China) and with the steady-state Xe900 450 W xenon lamp as the excitation source, TiO_2 as a work electrode, a Pt wire as a counter electrode and an Ag/AgCl (saturated KCl) as the reference electrode dipped in a solution of 0.5 M H_2SO_4 (scan rate: 50 mV/s).

2.3. Positron lifetime spectroscopy measurement

The slow positron annihilation spectroscopy used the mono-energetic slow positron beam generated from Na radioactive source with the energy ranging from 0.5 to 20 keV as lattice probe. Doppler broadening of annihilation radiation was estimated using an HPGe detector with a 0.2% energy resolution.

3. Results and discussion

3.1. Structure and morphology

Fig. 1 shows the X-ray diffraction (XRD) of TiO_2 on the fluorine doped tin oxide (FTO) substrate with different annealing temperature. Peaks indicated as circles are from FTO substrate. Since we have used the same methods with the previous work [16] and they had a same peak from XRD, it can concluded that the indicated diffraction peaks patterns in unannealed TiO_2 can be attributed to hexagonal $TiOF_2$, the indicated diffraction peaks in annealed TiO_2 can be attributed to the anatase TiO_2 exposed with the {116} facets. The intensities of the characteristic peaks increased obviously with

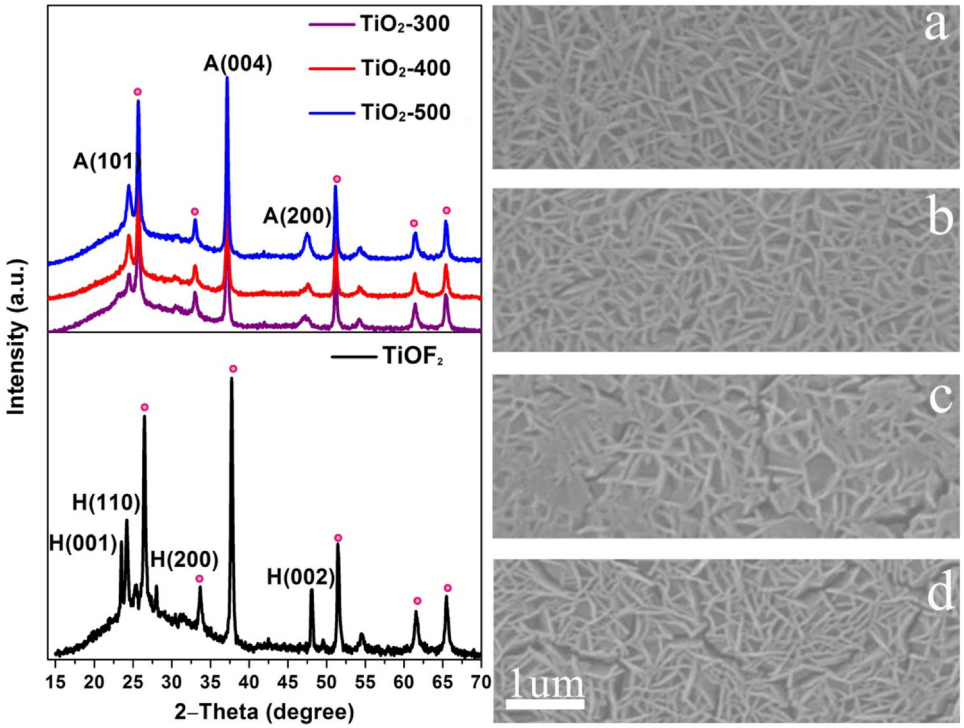

Fig. 1. XRD patterns and SEM images of the samples of (a) $TiOF_2$, (b) TiO_2-300, (c) TiO_2-400, and (d) TiO_2-500, respectively.

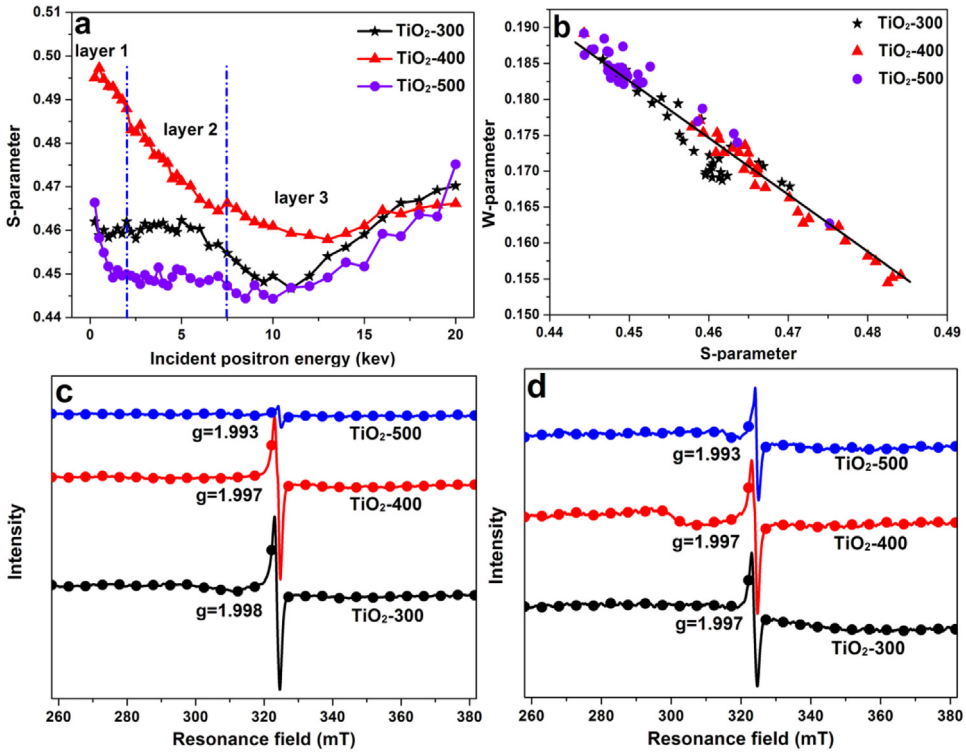

Fig. 2. The S-parameter as a function of positron implantation energy (a), the dependence of W and S parameters (b), electron paramagnetic resonance spectra (c) and electron paramagnetic resonance spectra under light (d) for TiO_2 annealed at 300 °C, 400 °C, 500 °C respectively.

the increase of the annealing temperature, which indicated that the sample of TiO_2-500 has the highest degree of crystallinity.

The SEM images of $TiOF_2$ and TiO_2 annealed at 300, 400 and 500 °C are shown in Fig. 1. It shows that they have similar nanosheet array structures after annealed at different temperature, which due to the precursor plays a hard template role for the growth of the nanosheet [16]. Moreover, the nanosheets cross into each other, which will prevent the nanosheet array from aggregating or collapsing. And those TiO_2 nanosheet array were collected with {116} facets parallel to the surface based on the previous results [13].

3.2. Defect analysis

As a unique nondestructive probe, positron annihilation technique has been used to detect the vacancy-type defects in the samples. Positrons have a high tendency to be captured by vacancy defects, which leads to a narrowing of the 511 keV annihilation peak contrast with bulk annihilation. The line-shape parameters S and W can be used to measure the Doppler broadening of the annihilation peak. The S/W is defined as a fraction of counts in the central area and in the wing area of the annihilation peak, respectively [21]. Therefore, positrons trapped in vacancy defects will result in an increase in S and a decrease in W, and each type of defect will exhibit its own S and W parameter. Thus, if only one type of defects is innovated, S will depends linearly on W [22].

S-parameter as a function of incident positron energy is shown in Fig. 2a. Based on VEPFIT analyses, the plots can be divided into three layers. In layer I, positron between the energy ranged of 0.25–2 keV annihilates at the surface of nanosheets. In layer II, energy range between 2 and 7.5 keV is looked upon the inner feature of nanosheets. The increases of S parameters in layer II demonstrates the emersion of cation related vacancies defects after annealing. In layer III, the positrons with the incident energy above 7.5 keV annihilated mainly in the substrate and the plots overlapped. Moreover, the S parameters in layer II shows apparent increase with annealing from 300 °C to 400 °C and then decrease to minimum value after further annealing at 500 °C. These results indicates that TiO_2 nanosheets with different defects concentration have been gotten by annealed at different temperatures.

In order to check the type of defect species in layer II, we also give out the S–W analysis for all the annealed samples as shown in Fig. 2b. The surface points with the positron energy below 2 keV were removed from all the S–W data. The straight lines of S–W data are observed in the annealed samples which indicate that only one type of defects exist in these samples. And the type of defects in layer II of these samples is considered mainly to be Ti related vacancies inside the nanosheets, as the cation vacancies as dominant positron trapping defects generally exist in materials. However, the positron lifetime spectra only apply to bulk samples, the defect type of TiO_2 nanosheets film could not identified by the positron measurement.

EPR and XPS technique were employed to analyze the defect types. From Fig. 2c, there are obvious signals at g = 1.99 for the samples annealed at different temperature. The signals at g = 1.99 can be attributed to Ti^{3+} [23,24]. Therefore the defect probed from slow positron annihilation spectroscopy may be considered to Ti^{3+} related vacancy which is consisted with the prediction. Ti^{3+} related vacancy defects mainly exists in the bulk lattice of the TiO_2 samples, then it can be considered as bulk defects, and the bulk defects increased with the annealing temperature first and then decreased when the annealing temperature increased to 500 °C. In the annealing process, a large number of oxygen vacancies generated and released electrons. These electrons are captured by Ti^{4+} and turn Ti^{4+} into Ti^{3+}, which has lower binding energy. With the change of annealing temperature, the EPR data of TiO_2-400 indicates that the sample annealed at 400 °C has the largest amount of Ti^{3+} related vacancy defects. The tendency is consistent to the result from the S–W analysis in layer II. Fig. 2d shows the EPR spectra measured under illumination, and it can be seen that the g values has no obvious change, although the peak intensity of TiO_2-500

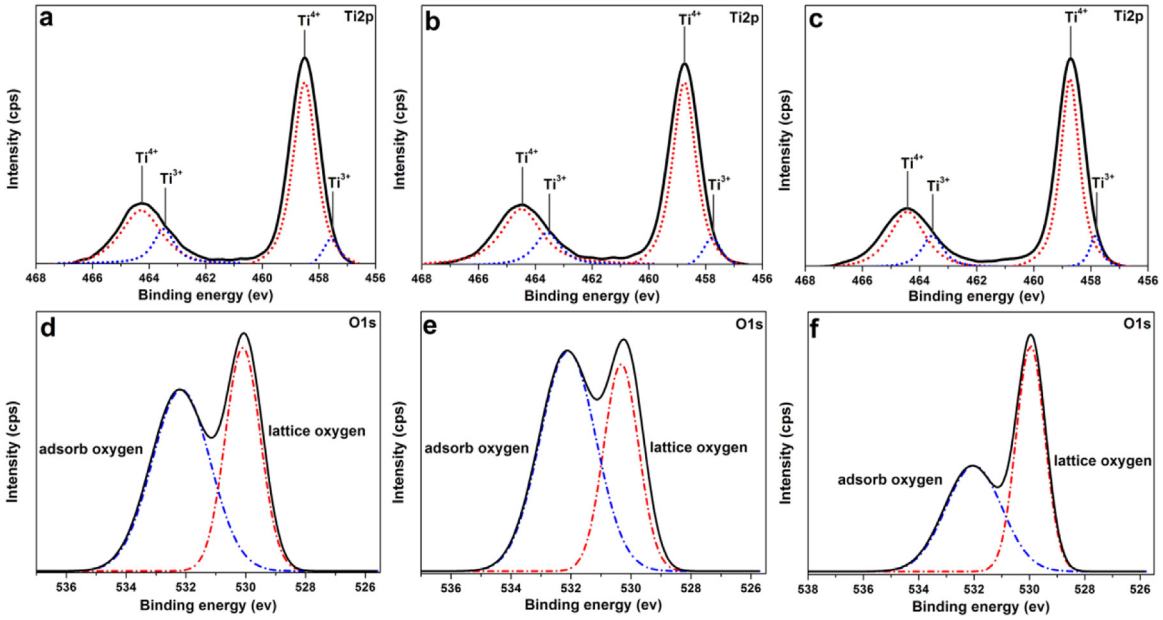

Fig. 3. XPS spectra of the samples (Ti 2p and O 1s): (a, d) TiO_2-300, (b, e) TiO_2-400, and (c, f) TiO_2-500 films respectively.

improved obviously, which means that TiO_2-500 has generated more unpaired electrons under illumination than other films. When photons with energy equal to or larger than the band gap are absorbed by TiO_2, electrons are excited from the valence band to the conduction band, creating electron-hole pairs. Electron-hole pairs tend to recombination within the semiconductor inside or surface, releasing heat, light, or other forms of energy. TiO_2-400 has the most Ti^{3+} related vacancy that will hinder the migration of electronic and lead to the recombination of electron-hole pairs, so it has less unpaired electrons.

Fig. 3 displays the XPS spectra of Ti 2p, and O 1s for the TiO_2 nanosheets films. The Gaussian functions are used in the curve resolution of the individual Ti 2p and O1s peaks. The Ti $2p_{1/2}$ and Ti $2p_{3/2}$ spin-orbital splitting photoelectrons for all samples locate at the binding energies 464 and 458 eV [25,26], and the peak of Ti^{3+}, Ti^{4+} are all gotten respectively, which proves the exist of Ti^{3+} that observed from EPR. Generally, O 1s spectra can be decomposed into two peaks: the first peak located at about 530 eV is assigned to lattice oxygen (Ti–O), while the shoulder peak at about 532 eV is assigned to adsorbed oxygen (Ti–OH) that can be seen as surface defects [27,28]. From Fig. 3, the surface defects added with the annealing temperature first and then decreased when the annealing temperature increased to 500 °C. The area of the peak Ti^{3+} related vacancy of samples is signed as S_{bulk}, while the area of adsorbed oxygen is signed as $S_{surface}$. Increasing the temperature from 300 °C, 400 °C to 500 °C leads to a change of $S_{bulk}/S_{surface}$ from 1.09, 0.66–1.20, respectively, indicating that the relative concentration ratio of bulk defects to surface defects can be tuned by controlling the annealing temperature and the ratio of bulk defects to surface defects reduced with the raised temperature and then increased. Furthermore, calcination of TiO_2 at 400 °C has the smallest values of $S_{bulk}/S_{surface}$, through very high concentration of bulk defects and surface defects in TiO_2-400.

3.3. Photocurrent measurements

To investigate the relation between the defects and photogenerated electron-hole of TiO_2-300, TiO_2-400 and TiO_2-500 films, the photocurrent measurements were performed under Xe lamp irradiation with bias potential of 0 and 0.5 V as shown in Fig. 4(a, b). It is known that the photocurrent depend on the electron-hole separation efficiency, thus the higher the electron-hole separation efficiency is accompanied by higher photocurrent and photocatalytic activity [3]. The photocurrent value at bias 0.5 V changed with the values of $S_{bulk}/S_{surface}$ was shown in Fig. 4c. It can be seen from Fig. 4c, the electron-hole separation efficiency increases with the increasing of $S_{bulk}/S_{surface}$ in the TiO_2 nanosheet films. The maximum photocurrent with bias potential of 0.5 V for TiO_2-500 is 4.1, 7.1 times higher than those of TiO_2-300 and TiO_2-400, respectively. TiO_2-400 has the lowest photocurrent, which indicates the most serious recombination. Considered the lowest $S_{bulk}/S_{surface}$ value TiO_2-400 has, photogenerated charge carriers may be rapidly trapped on the surface defects and recombined. Thus, TiO_2-500 with the highest $S_{bulk}/S_{surface}$ could significantly decrease the recombination of photogenerated electron-hole on surface, and display the highest photocurrent. All the above results show that changing the relative concentration ratio of bulk defects to surface defects could modify the electron-hole separation efficiency of the TiO_2 nanosheets films. Compared with Fig. 4(a) and (b), it can see that the photocurrent increase synchronically with the increase of the potential. The higher the bias, the higher photocurrent is.

In order to understand the photocatalysis process deeply, the photodegradation effects are shown in Fig. 4d. As shown in Fig. 4d, all of the TiO_2 samples exhibit a much higher photodegradation rate than $TiOF_2$. The photodegradation rate of TiO_2-500 is 1.1 and 1.2 times higher than those of TiO_2-300 and TiO_2-400, respectively. Therefore, the higher $S_{bulk}/S_{surface}$, the higher photodegradation rate is. In other words, the existence of surface adsorbed oxygen, have a negative effect on the photodegradation rate. TiO_2-500 and TiO_2-300, which are with the higher $S_{bulk}/S_{surface}$ than TiO_2-400, demonstrates the higher photodegradation rate, meaning that increasing $S_{bulk}/S_{surface}$ can improve the photocatalytic activity obviously. Based on the photocurrent performance, the improvement of photocatalytic efficiency is ascribed to the great enhancement of electron-hole separation efficiency, which is realized by increasing $S_{bulk}/S_{surface}$ of the TiO_2 nanosheet films.

PL spectra were also used to study the recombination and separation of electron-hole in the films. Fig. 5 shows that the PL intensity increases and then decreases when the temperature increased, TiO_2-400 has the strongest PL intensity, which evidence that most

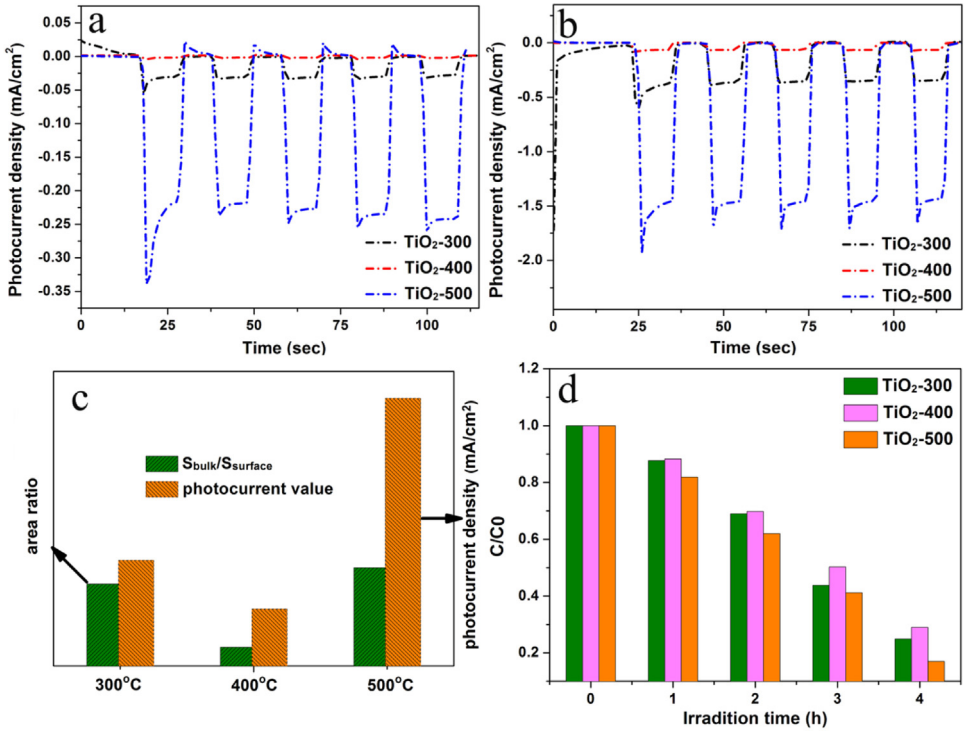

Fig. 4. (a, b) Photocurrent versus time (*I*–*t*) curves at a bias potential of 0 V and 0.5 V versus Ag/AgCl, (c) $S_{bulk}/S_{surface}$ and photocurrent value at 0.5 V at different temperature and (d) time courses for photocatalytic degradation of RhB.

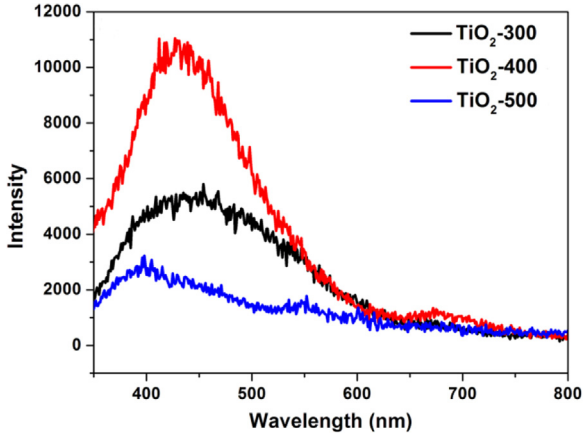

Fig. 5. PL spectra excitation at 300 nm of TiO_2-300, TiO_2-400 and TiO_2-500 nanosheet films.

of electrons and holes priority used for recombination luminescence in TiO_2-400. Base on above analysis, TiO_2-400 have the lowest $S_{bulk}/S_{surface}$, which leads to electrons and holes recombination more than separation. This demonstrated again that the surface adsorbed oxygen suppressed the separation and migration of electron-hole, therefore reduce the photocatalytic activity of TiO_2-400.

4. Conclusion

In summary, defects in TiO_2 nanosheet films play important roles in photocatalysis. Changing their concentration ratio of bulk/surface defects in TiO_2 nanosheet films improves the electron-hole separation efficiency significantly, thus enhances the photocatalytic efficiency significantly. By combining positron annihilation spectroscopy, EPR and XPS, we firstly concluded that the bulk defects are belonging to Ti^{3+} related vacancy defects. The results show that the redundant surface adsorbed oxygen, could subdue the separation and migration of electron-hole and reduce the photocatalysis efficiency.

Acknowledgments

This work was financially supported by the National Key Research and Development Program of China (2016YFA0401004), the External Cooperation Program of BIC, Chinese Academy of Sciences (211134KYSB20130017), Key Research Program of Chinese Academy of Sciences (KGZD-EW-T06), State Key Laboratory of Particle Detection and Electronics, University of Science and Technology of China and the Hefei Science Center CAS (2016HSC-IU004).

References

[1] X. Chen, S.S. Mao, Titanium dioxide nanomaterials: synthesis, properties, modifications, and applications, Chem. Rev. 107 (2007) 2891–2959.
[2] D. Beydoun, R. Amal, G. Low, S. McEvoy, Role of nanoparticles in photocatalysis, J. Nanopart. Res. 1 (1999) 439–458.
[3] M. Kong, Y.Z. Li, X. Chen, T.T. Tian, P.F. Fang, F. Zheng, X.J. Zhao, Tuning the relative concentration ratio of bulk defects to surface defects in TiO_2 nanocrystals leads to high photocatalytic efficiency, J. Am. Chem. Soc. 133 (2011) 16414–16417.
[4] G. Mattioli, F. Filippone, P. Alippi, A.A. Bonapasta1, Ab initio study of the electronic states induced by oxygen vacancies in rutile and anatase TiO_2, Phys. Rev. B 78 (2008) 241201.
[5] Y.B. He, O. Dulub, H.Z. Cheng, A. Selloni, U. Diebold, Evidence for the predominance of subsurface defects on reduced anatase TiO_2 (101), Phys. Rev. Lett. 102 (2009) 106105.
[6] X.Q. Gong, A. Selloni, M. Batzill, U. Diebold, Steps on anatase TiO_2 (101), Nat. Mater. 5 (2006) 665–670.
[7] J. Lee, D.C. Sorescu, X.Y. Deng, Electron-induced dissociation of CO_2 on TiO_2 (110), J. Am. Chem. Soc. 133 (2011) 10066–10069.
[8] E. Lira, S. Wendt, P. Huo, J. Hansen, R. Streber, S. Porsgaard, Y.Y. Wei, R. Bechstein, E. Lægsgaard, F. Besenbacher, The importance of bulk Ti^{3+} defects in the oxygen chemistry on titania surfaces, J. Am. Chem. Soc. 133 (2011) 6529–6532.

[9] X.F. Cui, B. Wang, Z. Wang, T. Huang, Y. Zhao, J.L. Yang, J.G. Hou, Formation and diffusion of oxygen-vacancy pairs on TiO_2 (110)-(1 × 1), J. Chem. Phys. 129 (2008) 044703.
[10] R.K. Singhal, Sudhish Kumar, P. Kumari, Y.T. Xing, E. Saitovitch, Evidence of defect-induced ferromagnetism and it switch action in pristine bulk TiO_2, Appl. Phys. Lett. 98 (2011) 092510.
[11] Prashun Gorai, Alice G. Hollister, Edmund G. Seebauer, Electrostatic drift effects on near-surface defect distribution in TiO_2, Appl. Phys. Lett. 103 (2013) 141601.
[12] J. Yan, G. Wu, N. Guan, et al., Understanding the effect of surface/bulk defects on the photocatalytic activity of TiO_2: anatase versus rutile, Phys. Chem. Chem. Phys. 15 (2013) 10978–10988.
[13] S.B. Wang, L. Pan, J.J. Song, W.B. Mi, J.J. Zou, L. Wang, X.W. Zhang, Titanium-defected undoped anatase TiO_2 with p-type conductivity room-temperature ferromagnetism, and remarkable photocatalytic performance, J. Am. Chem. Soc. 137 (2015) 2975–2983.
[14] L. Pan, S.B. Wang, J.W. Xie, L. Wang, X.W. Zhang, J.J. Zou, Constructing TiO_2 pn homojunction for photoelectrochemical and photocatalytic hydrogen generation, Nano Energy 28 (2016) 296–303.
[15] L. Pan, S.B. Wang, J.J. Zou, Z.F. Huang, L. Wang, X.W. Zhang, Ti^{3+}-defected and V-doped TiO_2 quantum dots loaded on MCM-41, Chem. Commun. 50 (2014) 988–990.
[16] F. Li, J. Xu, L. Chen, B.B. Ni, X.N. Li, Z.P. Fu, Y.L. Lu, Nanosheet array assembled by TiO_2 nanocrystallites with {116} facets parallel to the nanosheet surface, J. Mater. Chem. A. 1 (2013) 225–228.
[17] F. Li, X.N. Li, S.F. Yang, Z.P. Fu, Y.L. Lu, Tailoring of {116} faceted single crystalline anatase nanosheet arrays and their improved electrochemical performance, Cryst. Eng. Commun. 17 (2015) 4377–4382.
[18] F. Li, X.N. Li, R.R. Peng, X.F. Zhai, S.F. Yang, Z.P. Fu, Y.L. Lu, {116} faceted anatase single-crystalline nanosheet arrays: facile synthesis and enhanced electrochemical performances, Nanoscale 6 (2014) 12434–12439.
[19] X.J. Wu, P. Liu, L. Ma, J. Zhou, Y.S. Chen, J.X. Lu, S.-E. Yang, Two-dimensional modeling of TiO_2 nanowire based organic–inorganic hybrid perovskite solar cells, Sol. Energy Mater. Sol. C 152 (2016) 111–117.
[20] X. Wang, S.A. Kulkarni, Z. Li, et al., Wire-shaped perovskite solar cell based on TiO2 nanotubes, Nanotech 27 (2016) 20LT01.
[21] J. Toivonen, T. Hakkarainen, M. Sopanen, H. Lipsanen, J. Oila, K. Saarinen, Observation of defect complexes containing Ga vacancies in GaAsN, Appl. Phys. Lett. 82 (2003) 40–42.
[22] J. Gebauer, F. Borner, R. Krause-Rehberg, T.E.M. Staab, W. Bauer-Kugelmann, G. Kogel, W. Triftshauser, P. Specht, R.C. Lutz, E.R. Weber, M. Luysberg, Defect identification in GaAs grown at low temperatures by positron annihilation, J. Appl. Phys. 87 (2000) 8368–8379.
[23] J.C. Conesa, J. Soria, Reversible titanium (3 +) formation by hydrogen adsorption on M/anatase (TiO_2) catalysts, J. Phys. Chem. 86 (1982) 1392–1395.
[24] I. Nakamura, N. Negishi, S. Kutsuna, T. Ihara, S. Sugihara, K. Takeuchi, Role of oxygen vacancy in the plasma-treated TiO_2 photocatalyst with visible light activity for NO removal, J. Mol. Catal. A: Chem. 161 (2000) 205–212.
[25] Q. Liu, X. Wu, B. Wang, Q. Liu, Preparation and super-hydrophilic properties of TiO_2/SnO_2 composite thin films, Mater. Res. Bull. 37 (2002) 2255–2262.
[26] T. Ohsaka, F. Izumi, Y. Fujiki, Raman spectrum of anatase, TiO_2, J. Raman Spectrosc. 7 (1978) 321–324.
[27] M. Zhou, J. Yu, B. Cheng, H. Yu, Preparation and photocatalytic activity of Fe-doped mesoporous titanium dioxide nanocrystalline photocatalysts, Mater. Chem. Phys. 93 (2005) 159–163.
[28] M. Kang, M.H. Lee, Synthesis and characterization of Al- Bi-, and Fe-incorporated mesoporous titanosilicate (MPTS) materials and their hydrophilic properties, Appl. Catal. A 284 (2005) 215–222.